Nonlinear effects in pulse propagation through Doppler-broadened closed-loop atomic media

Robert Fleischhaker* and Jörg Evers†
Max-Planck-Institut für Kernphysik, Saupfercheckweg 1, D-69117 Heidelberg, Germany
(Received 26 November 2007; published 3 April 2008)

Nonlinear effects in pulse propagation through a medium consisting of four-level double-Λ-type systems are studied theoretically. We apply three continuous-wave driving fields and a pulsed probe field such that they form a closed interaction loop. Due to the closed loop and the finite frequency width of the probe pulses, the multiphoton resonance condition cannot be fulfilled, such that a time-dependent analysis is required. By identifying the different underlying physical processes we determine the parts of the solution relevant to calculate the linear and nonlinear response of the system. We find that the system can exhibit a strong intensity-dependent refractive index with small absorption over a range of several natural linewidths. For a realistic example we include Doppler and pressure broadening and calculate the nonlinear self-phase modulation in a gas cell with sodium vapor and argon buffer gas. We find that a self-phase modulation of π is achieved after the propagation of a few centimeters through the medium while the absorption and pulse shape distortion in the corresponding spectral range is small.

DOI: 10.1103/PhysRevA.77.043805 PACS number(s): 42.50.Gy, 42.65.Sf, 42.65.An, 32.80.Wr

I. INTRODUCTION

A main interest in laser-driven atomic media is the study of their coherence properties. Coherence effects like electromagnetically induced transparency (EIT) [1], coherent population trapping [2], lasing without inversion [3], and others [4,5] are examples where the optical properties of an atomic medium are influenced by coherent fields. The interference of different excitation channels is the main underlying principle here. A particular class of systems in which quantum mechanical interference plays a major role are the so-called closed-loop systems [6–17]. In these systems the laser-driven transitions form a closed interaction loop such that photon emission and absorption can take place in a cycle. This leads to interference of indistinguishable transition pathways between different states. One consequence of this is that it can render the system dependent on the relative phase of the driving fields. At the same time, however, the investigation of closed-loop systems is made difficult by the fact that the interfering pathways typically prevent the system from reaching a time-independent steady state. Such a stationary state in general is only reached when the so-called multiphoton resonance condition on the detunings of the different driving field is fulfilled, which was therefore assumed in most previous studies. For general laser field detunings, a time-dependent analysis is mandatory [8,11].

Laser-driven atomic media are also known to exhibit significant nonlinear optical properties [10–30]. A particular example is the occurrence of an intensity-dependent refractive index, with applications such as beam focusing, pulse compression, self-phase or cross-phase modulation, or optical switching [23–30]. Here, the connection to coherence properties is the following. While an atomic resonance can greatly enhance nonlinear effects in atomic media, the accompanying linear absorption of the same resonance typically renders the medium opaque to the probe field. This can be overcome by tailoring the response via coherence and interference effects. An advantageous situation arises, e.g., if the linear absorption vanishes due to destructive interference while the nonlinear effect is enhanced by constructive interference.

Motivated by this, we investigate nonlinear effects in pulse propagation through a closed-loop atomic medium. In particular, we study a four-level atomic system where the four dipole-allowed transitions form a double-Λ-type scheme (see Fig. 1). Three of the fields are assumed to be continuous-wave coupling laser fields, while the fourth field is a pulsed probe field. We use a time-dependent analysis, as the multiphoton resonance condition cannot be applied due to the finite-frequency spectrum of the probe pulses. The medium is modeled as a dilute gas vapor including Doppler

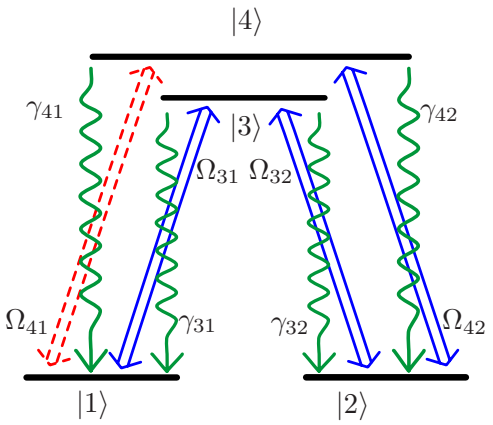

FIG. 1. (Color online) The four-level atomic system with the four dipole-allowed transitions forming a closed-loop double-Λ-type scheme. Three transitions are driven by continuous-wave control fields indicated by the solid blue double arrows. The fourth transition couples to the pulsed probe field indicated by the dashed red double arrow. The coupling strengths are given by the Rabi frequencies Ω_{jk}. The spontaneous decays with rates γ_{jk} are denoted by the wiggly green lines ($j \in \{3,4\}$, $k \in \{1,2\}$).

*robert.fleischhaker@mpi-hd.mpg.de
†joerg.evers@mpi-hd.mpg.de

and pressure broadening and an additional buffer gas using realistic parameters. Our main observable is the nonlinear index of refraction of the medium. We find that our system exhibits a high nonlinear index of refraction with small linear and nonlinear absorption over a spectral range of several natural linewidths. In this spectral region of interest, group velocity dispersion is low, such that pulse shape distortions are minimized. For sodium atoms with argon buffer gas, we obtain a nonlinear self-phase modulation of π after 6.4 cm of passage through the medium.

The paper is organized as follows. In Sec. II A we present our model. In Sec. II B we solve for the time-dependent long-time limit arising from the closed interaction loop in the form of a series. The interpretation of the series coefficients with respect to their physical meaning (Sec. II C) will enable us to identify the quantities necessary to calculate the linear and nonlinear susceptibility for the probe field of our system (Sec. II D). Doppler and pressure broadening are discussed in Secs. II E and II F. Our results are presented in Sec. III, both with and without broadening. Finally, Sec. IV discusses and summarizes our results.

II. THEORETICAL ANALYSIS

A. Model

In this section we present the Hamiltonian for the four-level system and the interaction with the coupling fields in a suitable interaction picture. We write the field coupling to transition $|j\rangle \leftrightarrow |k\rangle$ ($j \in \{3,4\}$, $k \in \{1,2\}$) as

$$\boldsymbol{E}_{jk} = \frac{E_{jk}}{2}(\hat{\boldsymbol{e}}_{jk} e^{-i\omega_{jk}t} + \text{c . c.}), \tag{1}$$

with amplitude E_{jk}, unit polarization vector $\hat{\boldsymbol{e}}_{jk}$, and frequency ω_{jk}. For better readability we suppress the space dependence of the fields. The Hamiltonian in dipole and rotating-wave approximation reads [4,5]

$$H = \sum_{j=1}^{4} \hbar\omega_j A_{jj} - \sum_{j=3}^{4}\sum_{k=1}^{2} \frac{\hbar\Omega_{jk}}{2}\{e^{-i(\omega_{jk}t-\phi_{jk})}A_{jk} + \text{H.c.}\}. \tag{2}$$

The energy of level $|j\rangle$ is denoted by $\hbar\omega_j$, and we have introduced the Rabi frequencies $\Omega_{jk} = E_{jk}|\hat{\boldsymbol{e}}_{jk}\boldsymbol{d}_{jk}|/\hbar$ with $\boldsymbol{d}_{jk}$ being the dipole matrix element of transition $|j\rangle \leftrightarrow |k\rangle$ ($j \in \{3,4\}$, $k \in \{1,2\}$). The complex phase of the Rabi frequencies was included in the exponential function where $\phi_{jk} = \arg(\hat{\boldsymbol{e}}_{jk}\boldsymbol{d}_{jk})$. The atomic transition or projection operator is defined as $A_{jk} = |j\rangle\langle k|$.

The canonical approach with a Hamiltonian of the sort we have just introduced would be to transform it into an interaction picture where the time dependence fully vanishes. Unfortunately, this is not possible in our case. Due to the closed interaction loop, in general a residual time dependence in the Hamiltonian remains. Physically, this means that we cannot expect the system to reach a true stationary state in the long-time limit. The best we can do is to use a unitary transformation that gathers all the time dependence in a single exponential factor in front of the probe field Rabi frequency. In this interaction picture we obtain

$$\begin{aligned} H_I = {} & \hbar(\Delta_{32} - \Delta_{31})A_{22} - \hbar\Delta_{31}A_{33} + \hbar(\Delta_{32} - \Delta_{31} - \Delta_{42})A_{44} \\ & - \frac{\hbar}{2}(\Omega_{31}A_{31} + \Omega_{32}A_{32} + \Omega_{42}A_{42} \\ & + \Omega_{41}A_{41}e^{-i(\Delta t-\phi)} + \text{H.c.}), \end{aligned} \tag{3}$$

where the detunings are defined as $\Delta_{jk} = \omega_{jk} - (\omega_j - \omega_k)$. We have also defined the so-called multiphoton detuning and an equivalent combination of the dipole phases:

$$\Delta = \Delta_{41} + \Delta_{32} - \Delta_{31} - \Delta_{42}, \tag{4a}$$

$$\phi = \phi_{41} + \phi_{32} - \phi_{31} - \phi_{42}. \tag{4b}$$

The multiphoton detuning is a typical quantity characterizing a system with a closed interaction loop. Its significance will become more apparent in Sec. II C.

We now set up the master equation for the atomic density matrix ϱ. We include the unitary evolution due to the Hamiltonian in the interaction picture and relaxation dynamics due to spontaneous decay in a Born-Markov approximation. The collision-induced dynamics will be considered in Sec. II F. The unitary evolution is given by the von Neumann equation, and the spontaneous decay can be written in Lindblad form [4]. The master equation in the interaction picture then reads

$$\partial_t \varrho^I = \frac{1}{i\hbar}[H_I, \varrho^I] - \sum_{j=3}^{4}\sum_{k=1}^{2} \frac{\gamma_{jk}}{2}\{[\varrho^I A_{jk}, A_{kj}] + \text{H.c.}\}, \tag{5}$$

where ϱ^I is the density matrix in the interaction picture and γ_{jk} is the radiative decay rate of transition $|j\rangle \leftrightarrow |k\rangle$. For the further analysis we rewrite the master equation in a matrix-vector form. Because the trace of the density matrix is conserved, we use the corresponding condition

$$\text{Tr}\, \varrho^I = \sum_{j=1}^{4} \varrho^I_{jj} = 1 \tag{6}$$

to eliminate the diagonal element ϱ_{44}. Here, $\varrho^I_{jk} = \langle j|\varrho^I|k\rangle$. Introducing the vector $R = (\varrho^I_{11}, \varrho^I_{12}, \varrho^I_{13}, \ldots, \varrho^I_{43})^T$ containing the remaining 15 elements of the density matrix we find

$$\partial_t R + \Sigma = MR, \tag{7}$$

with an inhomogeneous part Σ that stems from the elimination of ϱ_{44} and a coefficient matrix M. Both Σ and M can be directly derived from the master equation (5) and contain the explicit time dependence arising from the time-dependent Hamiltonian (3). The explicit form of M and Σ is given in the Appendix.

B. Time-dependent solution

To treat the explicit time dependence of the equation of motion we first separate Σ and M into the time-independent part and the explicitly time-dependent part. For this, we define

$$\Sigma = \Sigma_0 + \Sigma_{-1}\Omega_{41}e^{i(\Delta t-\phi)} + \Sigma_1\Omega_{41}e^{-i(\Delta t-\phi)}, \tag{8a}$$

$$M = M_0 + M_{-1}\Omega_{41}e^{i(\Delta t-\phi)} + M_1\Omega_{41}e^{-i(\Delta t-\phi)}, \tag{8b}$$

with time-independent Σ_j and M_j ($j \in \{0, \pm 1\}$). We see that under the condition $\Delta = 0$ the explicit time dependence vanishes. This is the so-called multiphoton resonance condition. For fixed coupling field frequencies this condition can only be fulfilled for a single probe field detuning Δ_{41}. But we want to investigate probe fields consisting of pulses with finite temporal length, which due to the Fourier relations implies that a whole spectrum of probe field frequencies interacts with the medium at the same time. Thus, we cannot assume the multiphoton resonance condition to be fulfilled [8]. Instead, we have to solve Eq. (7) including the explicit time dependence. To do so, we expand R as a power series in Ω_{41}:

$$R = \sum_{n=0}^{\infty} R_n \Omega_{41}^n. \tag{9}$$

If we assume that the probe field strength is small compared to the control fields, this series will converge. Inserting Eqs. (8a), (8b), and (9) into Eq. (7), we can derive equations of motion for the individual coefficients R_n. To order $O(\Omega_{41}^n)$ we find

$$\partial_t R_n = M_0 R_n + \delta_{n,1}(\Sigma_{-1}e^{i(\Delta t-\phi)} + \Sigma_1 e^{-i(\Delta t-\phi)}) + (M_{-1}e^{i(\Delta t-\phi)} + M_1 e^{-i(\Delta t-\phi)})R_{n-1}. \tag{10}$$

This is an equation for R_n where the coefficient matrix M_0 is time independent and only the inhomogeneous part is time dependent. This time dependence is twofold, first again explicitly because of the exponential functions and second because of the dependence on R_{n-1}. Thus, we make an ansatz for the solution and write R_n in a Fourier series:

$$R_n = \sum_{m=-\infty}^{\infty} R_n^{(m)} e^{-im(\Delta t-\phi)}. \tag{11}$$

Projecting on the Fourier basis functions we derive a hierarchy of time-independent equations for the coefficients $R_n^{(m)}$. Up to order $O(\Omega_{41}^3)$ we find

$$R_0^{(0)} = M_0^{-1}\Sigma_0, \tag{12a}$$

$$R_1^{(\pm 1)} = (M_0 \pm i\Delta\mathbb{1})^{-1}(\Sigma_{\pm 1} - M_{\pm 1}R_0^{(0)}), \tag{12b}$$

$$R_2^{(0)} = -M_0^{-1}(M_{-1}R_1^{(1)} + M_1 R_1^{(-1)}), \tag{12c}$$

$$R_2^{(\pm 2)} = -(M_0 \pm 2i\Delta\mathbb{1})^{-1}M_{\pm 1}R_1^{(\pm 1)}, \tag{12d}$$

$$R_3^{(\pm 1)} = -(M_0 \pm i\Delta\mathbb{1})^{-1}(M_{\pm 1}R_2^{(0)} + M_{\mp 1}R_2^{(\pm 2)}), \tag{12e}$$

$$R_3^{(\pm 3)} = -(M_0 \pm 3i\Delta\mathbb{1})^{-1}M_{\pm 1}R_2^{(\pm 2)}, \tag{12f}$$

where $\mathbb{1}$ is the unit matrix and all other $R_n^{(m)}$ up to this order vanish. In general, we find that

$$R = \sum_{n=0}^{\infty} \sum_{\substack{m=-n,\\ -n+2,\ldots}}^{n} R_n^{(m)} \Omega_{41}^n e^{-im(\Delta t-\phi)}. \tag{13}$$

Since the Fourier coefficients $R_n^{(m)}$ in Eq. (12a)–(12f) only depend on the Fourier coefficients $R_{n-1}^{(m)}$ of the next lower order, the full solution can be calculated recursively.

C. Physical interpretation

To physically interpret the meaning of the different coefficients we study the influence of the different parts of the solution on the probe field. First, we write down the expansion series for the relevant probe field coherence in the Schrödinger picture ϱ_{41} using the explicit transformation relation connecting the Schrödinger picture with our interaction picture. We find

$$\varrho_{41} = \varrho_{41}^I e^{-i(\omega_{41}t-\phi_{41})}e^{i(\Delta t-\phi)}. \tag{14}$$

With ϱ_{41}^I given as component of the solution for R we find

$$\varrho_{41} = \sum_{n=0}^{\infty} \sum_{\substack{m=-n,\\ -n+2,\ldots}}^{n} [R_n^{(m)}]_{13}\Omega_{41}^n e^{-i[\omega_{41}+(m-1)\Delta]t}e^{i[\phi_{41}+(m-1)\phi]}, \tag{15}$$

where $[R_n^{(m)}]_{13}$ refers to the 13th component of the vector $R_n^{(m)}$. Thus, the coefficient $[R_n^{(m)}]_{13}$ gives a contribution at the probe field frequency ω_{41} plus a frequency shift of $(m-1)\Delta$. The corresponding physical process can be identified as follows. A combination of dipole phases $\phi = \phi_{41} - \phi_{42} + \phi_{32} - \phi_{31}$ indicates a full evolution through a loop which extends from state $|1\rangle$ to $|4\rangle$ and via $|2\rangle$ and $|3\rangle$ back to state $|1\rangle$. The transition direction is given by the sign of the corresponding dipole phase. The evolution around the interaction loop is also the physical reason for the frequency shift Δ of such a process. Altogether, $[R_n^{(m)}]_{13}$ represents a process with $(m-1)$-loop cycles where the sign of $m-1$ defines the direction, clockwise for positive or counterclockwise for negative sign. The remainder of the n probe transitions can be interpreted as direct transitions.

D. Linear and nonlinear susceptibility

With the above interpretation we can easily identify the parts of the solution leading to the linear and nonlinear susceptibility in the probe field. Because both contributions should oscillate at the probe field frequency, we see that $m=1$ must be fulfilled in Eq. (15). The order of Ω_{41} enables one to identify

$$\chi^{(1)}(\omega_{41}) \propto [R_1^{(1)}]_{13} \quad \text{at } O(\Omega_{41}^1), \tag{16a}$$

$$\chi^{(3)}(\omega_{41}) \propto [R_3^{(1)}]_{13} \quad \text{at } O(\Omega_{41}^3). \tag{16b}$$

There is no second-order contribution to the susceptibility as expected for an isotropic medium [18]. By comparing the microscopically calculated value for the polarization [4,5]

$$\boldsymbol{P}_{41} = N(\boldsymbol{d}_{14}\varrho_{41} + \text{c.c.}) \tag{17}$$

with the definition of the susceptibility [18],

$$\boldsymbol{P}_{41} = \varepsilon_0 \frac{E_{41}}{2}\left(\chi^{(1)} + \frac{3}{4}E_{41}^2\chi^{(3)}\right)\hat{\boldsymbol{e}}_{41}e^{-i\omega_{41}t} + \text{c.c.}, \tag{18}$$

we find

$$\chi^{(1)}(\omega_{41}) = \frac{3}{8\pi^2}\lambda_{41}^3 N\gamma_{41}[R_1^{(1)}]_{13}, \tag{19}$$

$$\frac{3}{4}E_{41}^2\chi^{(3)}(\omega_{41}) = \frac{3}{8\pi^2}\lambda_{41}^3 N\gamma_{41}\Omega_{41}^2[R_3^{(1)}]_{13}, \tag{20}$$

with ε_0 being the permittivity of free space, λ_{41} the wavelength of the probe field transition, and N the density of atoms in the gas.

We remark that $\chi^{(3)}(\omega_{41})=\chi^{(3)}(\omega=\omega_{41}-\omega_{41}+\omega_{41})$ is the lowest-order nonlinear contribution at the probe field frequency. It leads to an intensity-dependent refractive index that also depends on ω_{41} and can be different for each respective frequency of the probe pulse spectrum. This is not the case for other contributions to $\chi^{(3)}$. For example, $[R_0^{(0)}]_{13}$ oscillates at the frequency $\omega=\omega_{41}-\Delta$ and leads to a contribution $\chi^{(3)}(\omega=\omega_{31}-\omega_{32}+\omega_{42})$ (four-wave mixing). Here, the resulting frequency is independent of ω_{41}. Nevertheless, in principle those processes can influence the result for the linear and third-order susceptibility at certain probe field frequencies. For example, light can be scattered into the probe field mode via different processes. Whether this or similar contributions change the probe pulse depends on the pulse's frequency width compared to the multiphoton detuning Δ and more general also on the propagation direction of the probe field relative to the control fields. A definite answer to this question requires an analysis of the full pulse propagation dynamics through the medium which is beyond the scope of this work.

E. Doppler broadening

A typical experimental setup to investigate the coherence properties of a laser-driven atomic gas would be a gas cell with a dilute alkali-metal-atom vapor. For a dilute atomic gas theoretical predictions for the linear and nonlinear susceptibility can be made on the basis of a single atom analysis. This greatly facilitates the theoretical analysis. However, in a dilute gas at room temperature or above the atoms move at velocities where the frequency shift due to Doppler effect cannot be neglected compared to the natural linewidth given by the radiative decay rate γ. To calculate the Doppler effect for a single field, we assume a Maxwell-Boltzmann velocity distribution in laser propagation direction with a most probable velocity given by [32]

$$v_m = \sqrt{\frac{2k_BT}{m}}, \tag{21}$$

with k_B the Boltzmann constant, T the temperature, and m the mass of the atom. The nonrelativistic Doppler frequency shift is given by

$$\omega_{\text{eff}} = \omega\left(1 - \frac{v}{c}\right), \tag{22}$$

where ω_{eff} is the shifted frequency seen by the moving atom, ω is the laboratory frame laser frequency, v is the velocity of the atom in laser propagation direction, and c is the speed of light. The Doppler shift effectively leads to an additional detuning Δ_{Dop} with a Gaussian distribution [32]

$$f(\Delta_{\text{Dop}})d\Delta_{\text{Dop}} = \frac{1}{\sqrt{\pi}kv_m}e^{-(\Delta_{\text{Dop}}/kv_m)^2}d\Delta_{\text{Dop}}, \tag{23}$$

where k is the wave number. The corresponding linewidth [full width at half maximum (FWHM)] is then given by

$$\delta\omega = k\sqrt{\ln(2)\frac{8k_BT}{m}}. \tag{24}$$

To actually calculate the linear and nonlinear susceptibility for a Doppler-broadened medium, for each propagation direction, we have to add Δ_{Dop} to the detuning of the fields propagating in this direction and then average the resulting susceptibility over the velocity distribution (23).

F. Buffer gas and pressure broadening

Introducing a buffer gas to the gas cell leads to more frequent collisions between the atoms. This has two main consequences. First of all it causes pressure broadening. For moderate densities, a collision between two atoms disturbs the level energies for a short time which results in the loss of phase coherence. In a simple approach this can be modeled by an additional decay rate γ_c for the coherences. This collisional decay rate consists of a contribution due to the studied gas itself and a contribution due to the buffer gas. Both depend linearly on the respective densities N_s and N_b [18],

$$\gamma_c = C_sN_s + C_bN_b, \tag{25}$$

with gas specific constants C_s for the studied gas and C_b for the buffer gas.

A second major effect of a buffer gas is closely connected to Doppler broadening. Due to the higher density, the mean free path of a single atom moving in the gas is reduced. If it is reduced below the transition wavelength, an averaging over different velocities during a single emission or absorption process can effectively renarrow a Doppler-broadened line. This phenomenon is known as Dicke narrowing [31].

III. RESULTS

In principle, Eqs. (12a)–(12f) can be used to calculate analytical results for the desired $\chi^{(1)}$ and $\chi^{(3)}$. But in our situation of interest where all four electromagnetic fields, possibly all with different detuning, interact with the atom, these are usually too lengthy to give any physical insight. Therefore, we proceed with a numerical study of the linear and nonlinear susceptibility.

A. Without Doppler broadening

Here, our primary goal is to find a set of parameters where the intensity-dependent refractive index is large enough to

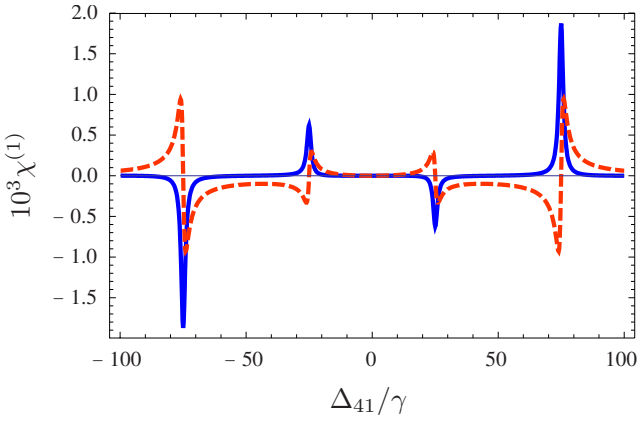

FIG. 2. (Color online) Real part (solid blue line) and imaginary part (dashed red line) of the linear susceptibility of the probe field. Due to strong control fields $\Omega_{42}=100\gamma$ and $\Omega_{31}=50\gamma$, the probe field resonance is split into four different resonances. Further, $\Omega_{32}=\Delta_{31}=\Delta_{32}=\Delta_{42}=0$ and all spontaneous decay rates γ_{jk} have been set to γ. The susceptibility is plotted in units of $3/8\pi^2\lambda_{41}^3 N_s$.

cause an appreciable amount of nonlinear self-phase modulation while the attenuation of a light pulse due to absorption is small. To achieve a high nonlinear index of refraction with low linear and nonlinear loss all in the same spectral region is challenging because resonances that enhance the nonlinear response typically come with strong absorption. Still, we find such a suitable parameter set by manipulating the linear and nonlinear susceptibility of the probe field as described next.

We first split the unperturbed resonance of the probe field transition by a strong coupling field Ω_{42} and again about half as much by the second coupling field Ω_{31}. This gives rise to four resonance structures in the linear response; see Fig. 2.

In this figure, the linear absorption of the resonance at $\Delta_{41}\approx-25\gamma$ can be lowered by a small detuning Δ_{31}, which modifies the dressed-state populations. Finally, optimizing the result with the third coupling Ω_{32}, we can tune one-half of the resonance to a small linear and nonlinear absorption while still maintaining a substantial nonlinear real part. In Fig. 3 it is shown how gradually introducing a detuning Δ_{31} influences the linear absorption, the nonlinear gain, and the real part of the nonlinear susceptibility. It decreases the linear absorption and the nonlinear gain faster than the real part and thereby improves their ratio. Interestingly, the imaginary parts of the linear and the nonlinear parts of the susceptibility can have opposite signs in this spectral region. The linear response induces absorption, while the nonlinear response leads to gain. Absorption could in this spectral region therefore be reduced even further by a partial canceling of linear absorption and nonlinear gain. However, these results are preliminary in the sense that no effects due to Doppler and pressure broadening have been included yet.

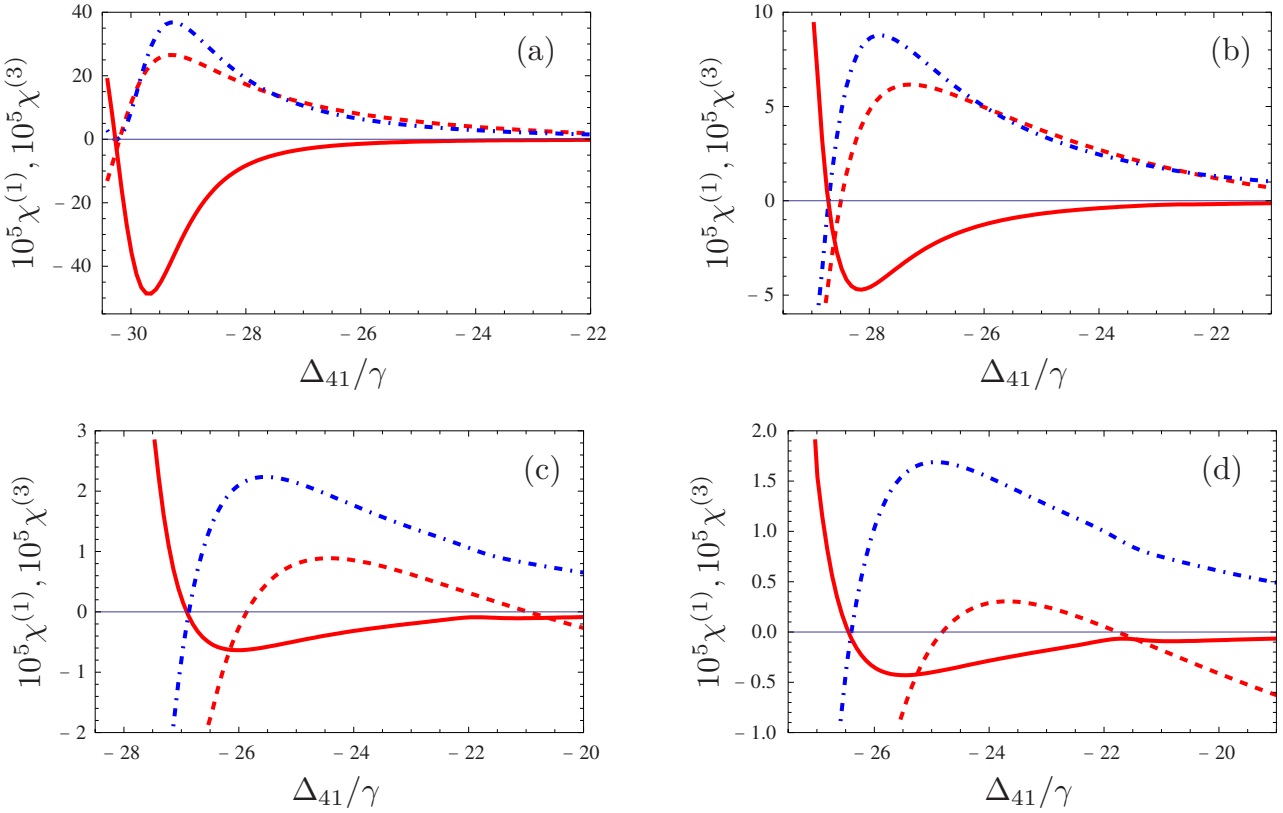

FIG. 3. (Color online) Real part (dash-dotted blue line) and imaginary part (solid red line) of the nonlinear susceptibility together with the imaginary part of the linear susceptibility (dashed red line). All figures show the resonance around $\Delta_{41}=-25\gamma$. The susceptibility is plotted in units of $3/8\pi^2\lambda_{41}^3 N$, and for comparability $\chi^{(3)}$ has been scaled with $3/4E_{41}^2$. The parameters are $\Delta_{32}=\Delta_{42}=0$, $\Omega_{31}=50\gamma$, $\Omega_{32}=34\gamma$, and $\Omega_{42}=100\gamma$. The probe field strength is assumed to be one-tenth of the weakest control field in all cases. The detuning Δ_{31} is chosen as (a) $\Delta_{31}=0$, (b) $\Delta_{31}=0.7\gamma$, (c) $\Delta_{31}=1.5\gamma$, and (d) $\Delta_{31}=1.7\gamma$. Note the different axis scales in the four subpanels.

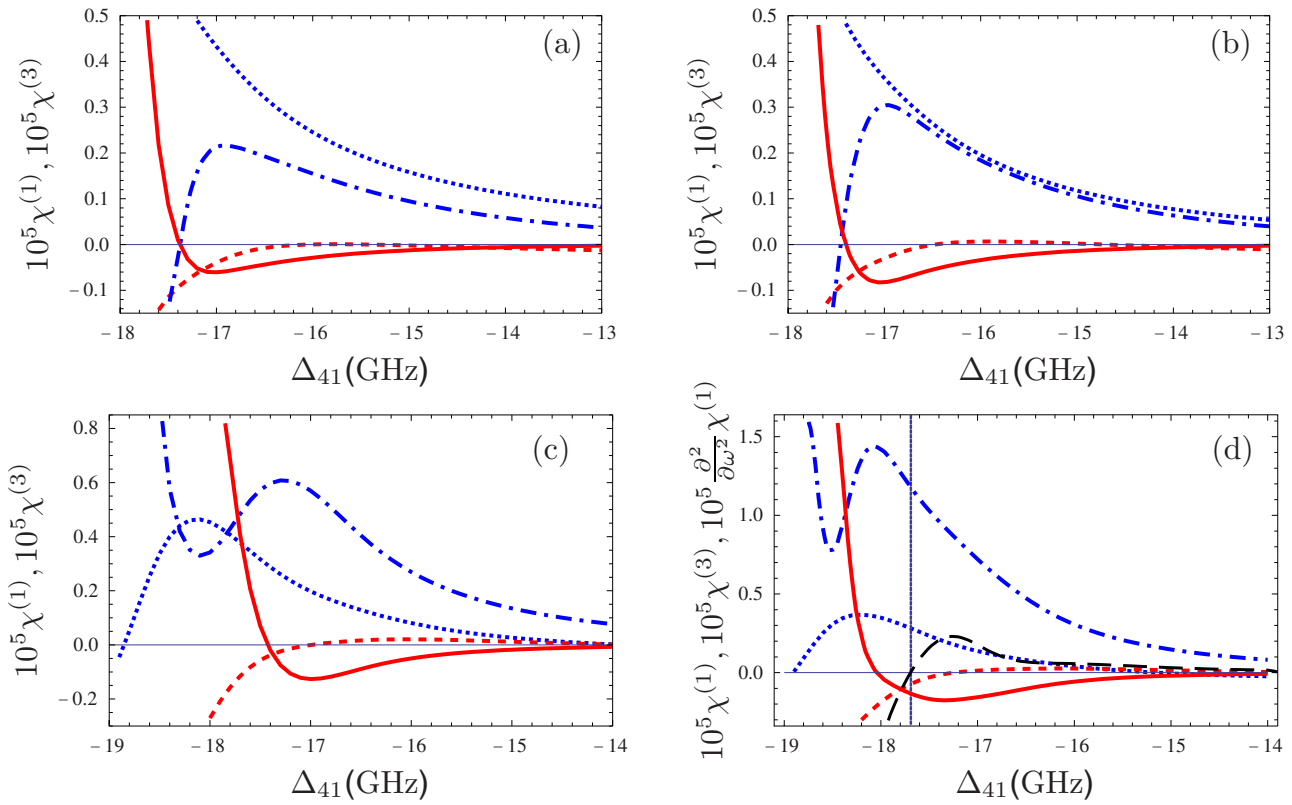

FIG. 4. (Color online) Real part (dash-dotted blue line) and imaginary part (solid red line) of the nonlinear susceptibility together with the real part (blue dotted line) and the imaginary part of the linear susceptibility (dashed red line) at the resonance around $\Delta_{41}=-15.0$ GHz. The control fields have Rabi frequencies $\Omega_{42}=60$ GHz, $\Omega_{31}=30$ GHz, and $\Omega_{32}=25$ GHz, and the detunings are $\Delta_{31}=1.6$ GHz and $\Delta_{32}=\Delta_{42}=0$. The medium parameters described in the main text correspond to sodium as the active medium with argon as a buffer gas. The four different plots show Doppler-averaged results with a Doppler linewidth of (a) below the natural linewidth, (b) 50%, (c) 90%, and (d) 100% of the full Doppler linewidth of $\delta\omega=2\pi\times 1.78$ GHz. In plot (d) we also included the second derivative of the real part of the linear susceptibility (long-dashed black line).

B. Including Doppler broadening

Using our considerations from Secs. II E and II F we now want to calculate the linear and nonlinear susceptibility in a Doppler-broadened atomic gas. As a realistic example, we want to assume a sodium vapor with a density of $N_s=1.0\times 10^{20}$ m^{-3}. To reach a vapor pressure that corresponds to this density the gas cell must be heated to a temperature of $T=547.6$ K [33]. At this temperature the Doppler linewidth is $\delta\omega=2\pi\times 1.78$ GHz which is very broad compared to the natural linewidth of the sodium D_1 transition of $\gamma=2\pi\times 9.76$ MHz. In a pure sodium vapor the spectral features we found in Sec. III A would be averaged out by the Doppler effect. But if we introduce a buffer gas, strong pressure broadening can preserve them. For sodium and argon, the gas parameters in Eq. (25) are given by $C_s=1.50\times 10^{-13}$ m^3 s^{-1} and $C_b=2.53\times 10^{-15}$ m^3 s^{-1} [18]. We want to assume a collision-induced coherence loss rate of $\gamma_c=1.0$ GHz which corresponds to a buffer gas density of $N_b=3.95\times 10^{23}$ m^{-3}. At such a density the mean free path is of order $\Lambda=10^{-5}$ m. This is much larger than the transition wavelength $\lambda=589.2\times 10^{-9}$ m such that the limit of Dicke narrowing is not reached.

We now try to recover results similar to the unbroadened case shown in Fig. 3. Because of the strong broadening, we have to apply correspondingly stronger control fields. For $\Omega_{42}=60.0$ GHz and $\Omega_{31}=30.0$ GHz, we find the resonance studied in the unbroadened case at around $\Delta_{41}=-15.0$ GHz. The third control field is set to $\Omega_{32}=25.0$ GHz and the detuning to $\Delta_{31}=1.6$ GHz. For the Doppler averaging we have assumed all fields to be copropagating. The different subpanels in Fig. 4 correspond to different Doppler linewidths and thus, via Eq. (24), to different temperatures. In Fig. 4(a), the Doppler linewidth is chosen below the natural linewidth of the probe transition, and as expected we find results that are similar in shape to the unbroadened case [see Fig. 3(d)]. The differences are mainly due to pressure broadening. In Figs. 4(b)–4(d) we gradually increase the Doppler linewidth up to the full Doppler width expected for the gas parameters discussed above. We find that while the shapes of the different curves change, our main result of high nonlinear index of refraction with small linear and nonlinear absorption persists with Doppler broadening. Also in the broadened case, a partial canceling of linear absorption and nonlinear gain could be possible. Note that since the averaging process affects not only the probe field detuning but all four detunings at the same time, the results cannot be explained in terms of a simple smoothing of the curves without the Doppler effect.

We also considered different laser geometries, such as control fields propagating perpendicular to the probe field, or

one or two control fields propagating in opposite directions, and found the copropagating case to be the most advantageous one. This is similar to the case of Doppler broadening in standard electromagnetically induced transparency setups where copropagating lasers typically are preferable.

We finally use our results to calculate the required optical length for a nonlinear self-phase modulation of π at a probe field frequency with vanishing group velocity dispersion. The group velocity dispersion is given by [4]

$$\beta_2 = \frac{k}{4}\frac{\partial^2 \mathrm{Re}[\chi^{(1)}]}{\partial \omega^2}, \tag{26}$$

where the wave vector k gives the characteristic length scale. The frequency of vanishing group velocity dispersion is thus given by the condition

$$\frac{\partial^2 \mathrm{Re}[\chi^{(1)}]}{\partial \omega^2} = 0, \tag{27}$$

which for the considered gas parameters yields

$$\Delta_{41}^{\min} = 17.63 \ \ \mathrm{GHz}. \tag{28}$$

This probe field frequency is indicated by the vertical solid blue line in Fig. 4(d).

The nonlinear self-phase modulation is given by [18]

$$\Delta\Phi_{\mathrm{NL}} = n_2 I k L, \tag{29}$$

with n_2 the intensity-dependent refractive index, I the probe field intensity, k the wave vector, and L the propagation length. We assume a probe field strength one-tenth of the smallest control field and find at frequency $\Delta_{41}^{\min}$:

$$L_\pi = 6.4 \ \ \mathrm{cm}. \tag{30}$$

From Fig. 4(d) we see that at $\Delta_{41}^{\min}$ the magnitude of the imaginary parts of the linear and nonlinear susceptibility is more than one order of magnitude smaller than the real part of the nonlinear susceptibility. Therefore, the equivalent characteristic length scale is more than one order of magnitude larger. Furthermore, both linear and nonlinear parts give rise to small gain rather than absorption.

To assess the frequency range in which the calculated nonlinear self-phase modulation length can be achieved without significant pulse shape distortion we in addition studied the group velocity dispersion. It is related via Eq. (26) to the second derivative of the real part of the linear susceptibility which is shown as the long-dashed black curve in Fig. 4(d). Figure 5 shows a magnification of Fig. 4(d) around $\Delta_{41}^{\min}$. We see that in a spectral range of several natural linewidth the second derivative of the real part of the linear susceptibility is about one order of magnitude smaller than the real part of the nonlinear susceptibility that is responsible for the nonlinear self-phase modulation. This suggests that a pulse with a bandwidth of up to several natural linewidth would suffer only little from group velocity dispersion on the calculated nonlinear self-phase modulation length.

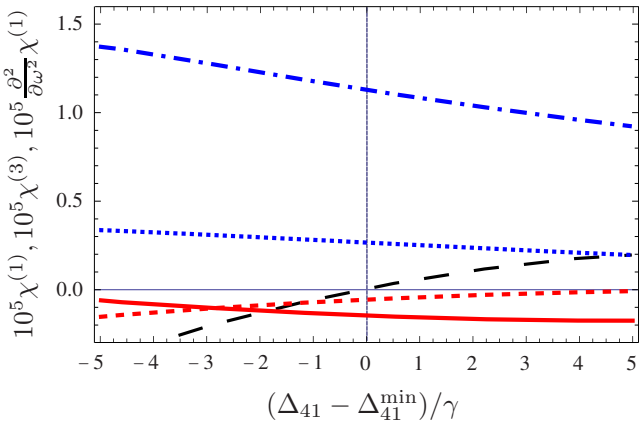

FIG. 5. (Color online) A magnification of Fig. 4(d) around the probe field frequency $\Delta_{41}^{\min}$ with vanishing group velocity dispersion [see Eq. (28)] is shown. The frequency axis is shown in units of the natural decay rate γ, which for the considered sodium $D1$ transition is $2\pi\times 9.76$ MHz. The parameters are the same as for Fig. 4(d).

For a more quantitative measure, we calculate the ratio of time spread to temporal width of a pulse with a bandwidth of x times the natural linewidth γ. The corresponding temporal width of the pulse is

$$\tau = \frac{2\pi}{x\gamma}. \tag{31}$$

The time spread of such a pulse is related to the parameter β_2 given by Eq. (26) in the following way [4]:

$$\Delta\tau = L\beta_2 x\gamma. \tag{32}$$

From Fig. 5, we estimate an average value of the second derivative of the real part of the linear susceptibility around $\Delta_{41}^{\min}$ of 0.2 (scaled quantity). For the ratio of $\Delta\tau$ and τ after a propagation length of L_π we find

$$\frac{\Delta\tau}{\tau} = \frac{1}{2\pi} L_\pi \beta_2 \gamma^2 x^2 \tag{33}$$

$$= 0.042 x^2. \tag{34}$$

Thus, the pulse doubles its temporal width for $x=4.9$. For longer pulses, x becomes smaller and this ratio improves with x^2.

Our results show that in a spectral range of several natural linewidths a nonlinear self-phase modulation of π can be achieved on a realistic laboratory length scale. We showed that in the same spectral range group velocity dispersion is low such that pulse shape distortions can be expected to be small. Interestingly, the real part of the linear susceptibility has a negative slope in the considered frequency region, in contrast to a positive slope typically found in an electromagnetically induced transparency window.

IV. CONCLUSION

We have studied nonlinear effects in pulse propagation through a laser-driven medium where the applied fields form

a closed interaction loop. Such loop systems in general only allow for a time-independent treatment at a single probe field frequency, where the so-called multiphoton resonance condition is fulfilled. As a probe field pulse has a finite frequency width, this condition, which allows for a straightforward theoretical treatment, could not be applied. Instead, we treated the time-dependent problem by turning it into a hierarchy of equations that describe the various physical processes occurring in the medium. We have included Doppler and pressure broadening as well as a buffer gas in our analysis and have used realistic parameters for a medium consisting of sodium vapor. We could show that the studied system can exhibit a high nonlinear refractive index with small absorption or gain over a spectral range of several natural linewidths. For the chosen parameters, group velocity dispersion is low, such that pulse shape distortions are minimized, and the slope of the linear dispersion is negative. A nonlinear self-phase modulation of π is obtained after 6.4 cm propagation through the medium.

APPENDIX: COEFFICIENT MATRIX

The explicit form of the coefficient matrix M and the inhomogeneous part Σ can be derived from Eq. (7). Here, we list all nonzero elements $M_{j,k}$ and Σ_j, which are given by

$$M_{1,1} = M_{1,6} = M_{6,6} = \frac{1}{2}M_{11,11} = \Sigma_1 = \Sigma_6 = -\gamma_r,$$

$$M_{1,3}^* = M_{1,9} = M_{2,10} = M_{3,4} = M_{4,12} = M_{5,7}^* = M_{9,11} = M_{13,15}^* = \frac{i}{2}\Omega_{31},$$

$$M_{2,3}^* = M_{5,9} = M_{6,7}^* = M_{6,10} = M_{7,11} = M_{8,12} = M_{10,11}^* = M_{14,15}^* = \frac{i}{2}\Omega_{32},$$

$$M_{1,4}^* = M_{1,13} = M_{2,14} = M_{3,15} = \frac{1}{2}M_{4,1}^* = M_{4,6}^* = M_{4,11}^* = M_{5,8}^* = M_{9,12}^* = \frac{1}{2}M_{13,1} = M_{13,6} = M_{13,11} = \Sigma_4^* = \Sigma_{13} = \frac{i}{2}\Omega_{41}e^{-i(\Delta t-\phi)},$$

$$M_{2,4}^* = M_{5,13} = M_{6,8}^* = M_{6,14} = M_{7,15} = M_{8,1}^* = \frac{1}{2}M_{8,6}^* = M_{8,11}^* = M_{10,12}^* = M_{14,1} = \frac{1}{2}M_{14,6} = M_{14,11} = \Sigma_8^* = \Sigma_{14} = \frac{i}{2}\Omega_{42},$$

$$M_{3,3} = M_{9,9}^* = -\gamma_r - i\Delta_{31},$$

$$M_{4,4} = M_{13,13}^* = -\gamma_r - i(\Delta_{31} + \Delta_{42} - \Delta_{32}),$$

$$M_{7,7} = M_{10,10}^* = -\gamma_r - i\Delta_{32},$$

$$M_{7,8} = M_{10,10} = -\gamma_r - i\Delta_{32},$$

$$M_{12,12} = M_{15,15}^* = -2\gamma_r - i(\Delta_{42} - \Delta_{32}),$$

$$M_{2,2} = M_{5,5}^* = -i(\Delta_{31} - \Delta_{32}),$$

$$M_{6,4} = M_{11,4} = M_{6,13} = M_{11,13} = M_{1,8} = M_{11,8} = M_{1,14} = M_{11,14} = 0,$$

where $M_{j,k}=M_{k,j}$ holds if not noted otherwise and by $M_{j,k}^*$ we indicate the complex conjugate of $M_{j,k}$.

[1] S. E. Harris, Phys. Today **50**(7), 36 (1997); M. Fleischhauer, A. Imamoglu, and J. P. Marangos, Rev. Mod. Phys. **77**, 633 (2005).

[2] G. Alzetta, A. Gozzini, L. Moi, and G. Orriols, Nuovo Cimento Soc. Ital. Fis., B **36**, 5 (1976); E. Arimondo, in *Progress in Optics*, edited by E. Wolf (Elsevier, Amsterdam, 1996), Vol. 35, p. 257.

[3] O. Kocharovskaya, Phys. Rep. **219**, 175 (1992).

[4] Z. Ficek and S. Swain, *Quantum Interference and Coherence: Theory and Experiments* (Springer, Berlin, 2005).

[5] M. O. Scully and M. S. Zubairy, *Quantum Optics* (Cambridge University Press, Cambridge, England, 1997).

[6] S. J. Buckle, S. M. Barnett, P. L. Knight, M. A. Lauder, and D. T. Pegg, Opt. Acta **33**, 2473 (1986); D. V. Kosachiov, B. G. Matisov, and Y. V. Rozhdestvensky, J. Phys. B **25**, 2473 (1992).

[7] V. S. Malinovsky and I. R. Sola, Phys. Rev. Lett. **93**, 190502 (2004).

[8] M. Mahmoudi and J. Evers, Phys. Rev. A **74**, 063827 (2006).

[9] W. E. van der Veer, R. J. J. van Diest, A. Donszelmann, and H. B. van Linden van den Heuvell, Phys. Rev. Lett. **70**, 3243 (1993).

[10] S. A. Babin, S. I. Kablukov, U. Hinze, E. Tiemann, and B. Wellegehausen, Opt. Lett. **26**, 81 (2001).

[11] W. Maichen, F. Renzoni, I. Mazets, E. Korsunsky, and L. Windholz, Phys. Rev. A **53**, 3444 (1996).

[12] E. A. Korsunsky and D. V. Kosachiov, Phys. Rev. A **60**, 4996 (1999).

[13] A. J. Merriam, S. J. Sharpe, M. Shverdin, D. Manuszak, G. Y. Yin, and S. E. Harris, Phys. Rev. Lett. **84**, 5308 (2000).

[14] G. Morigi, S. Franke-Arnold, and G. L. Oppo, Phys. Rev. A **66**, 053409 (2002).

[15] S. Kajari-Schröder, G. Morigi, S. Franke-Arnold, and G. L. Oppo, Phys. Rev. A **75**, 013816 (2007).

[16] A. F. Huss, R. Lammegger, C. Neureiter, E. A. Korsunsky, and L. Windholz, Phys. Rev. Lett. **93**, 223601 (2004).

[17] H. Shpaisman, A. D. Wilson-Gordon, and H. Friedmann, Phys. Rev. A **71**, 043812 (2005).
[18] R. W. Boyed, *Nonlinear Optics* (Academic Press, London, 1992).
[19] S. E. Harris, J. E. Field, and A. Imamoglu, Phys. Rev. Lett. **64**, 1107 (1990).
[20] P. R. Hemmer, D. P. Katz, J. Donoghue, M. Cronin-Golomb, M. S. Shariar, and P. Kumar, Opt. Lett. **20**, 769 (1995).
[21] D. A. Braje, V. Balic, S. Goda, G. Y. Yin, and S. E. Harris, Phys. Rev. Lett. **93**, 183601 (2004).
[22] M. D. Lukin, P. R. Hemmer, and M. O. Scully, Adv. At., Mol., Opt. Phys. **42**, 347 (2000).
[23] J. E. Bjorkholm and A. A. Ashkin, Phys. Rev. Lett. **32**, 129 (1974).
[24] H. Friedmann and A. D. Wilson-Gordon, Phys. Rev. A **52**, 4070 (1995).
[25] A. B. Matsko, I. Novikova, G. R. Welch, and M. S. Zubairy, Opt. Lett. **28**, 96 (2003).
[26] H. Schmidt and A. Imamoglu, Opt. Lett. **21**, 1936 (1996).
[27] S. E. Harris and L. V. Hau, Phys. Rev. Lett. **82**, 4611 (1999).
[28] T. Nakajima, Opt. Lett. **25**, 847 (2000).
[29] Y. P. Niu and S. Q. Gong, Phys. Rev. A **73**, 053811 (2006).
[30] T. N. Dey and G. S. Agarwal, Phys. Rev. A **76**, 015802 (2007).
[31] R. H. Dicke, Phys. Rev. **89**, 472 (1953).
[32] W. Demtröder, *Laser Spectroscopy: Basics Concepts and Instrumentation* (Springer, Berlin, 1996).
[33] D. A. Steck (unpublished).